

## Catalysts by design: genesis and CO hydrogenation of novel Pd carbonyl clusters in zeolite 5A

Zongchao Zhang, Fernando A.P. Cavalcanti and Wolfgang M.H. Sachtler

*V.N. Ipatieff Laboratory, Center for Catalysis and Surface Science, Northwestern University,  
Evanston, IL 60208, U.S.A.*

The potential of catalyst synthesis by design is demonstrated by comparing Pd/5A to Pd/NaY. While supercage dimensions are similar for both zeolites, the diameter of the supercage windows not only determines the Pd nuclearity of entrapped Pd carbonyl clusters, but also restricts their growth under CO hydrogenation conditions. While  $\text{Pd}_{13}(\text{CO})_x$  clusters prevail in zeolite Y as a result of migration and coalescence of primary Pd carbonyl clusters after CO exposure at room temperature, cluster growth in zeolite 5A is confined to  $\text{Pd}_6(\text{CO})_x$ . Under the conditions of syngas conversion, small Pd clusters are stabilized in the supercages of 5A, in contrast to the agglomeration of Pd particles to size larger than 60 Å in NaHY. The catalytic activity of Pd/5A is twice that of Pd/NaHY. The selectivities of CO hydrogenation on both catalysts are also drastically different: on Pd/5A, methanol and dimethylether are the sole products besides methane, but on Pd/NaHY, production of  $\text{C}_{2+}$  hydrocarbons is significant.

**Keywords:** CO hydrogenation; Pd carbonyl cluster; zeolite 5A

### 1. Introduction

Preparation and catalysis of zeolite encaged transition metal carbonyl clusters have been the subject of several studies [1,2]. However, it is only recently that a ship-in-a-bottle synthesis of  $\text{Pd}_{13}(\text{CO})_x$  clusters in zeolite Y has been successful [3–5]. In recent EXAFS characterization of Pd particles in zeolite Y after various pretreatment conditions, it was found that  $\text{Pd}_{13}(\text{CO})_x$  is a secondary product which results from the migration and coalescence of primary Pd carbonyl clusters at room temperature [6–8]. This agglomeration to clusters with a larger Pd core was shown to be irreversible; upon CO displacement by  $\text{H}_2$  at higher temperature, Pd particles increase to the size of the supercage or larger. CO hydrogenation on Pd/Y catalysts is, therefore, expected to proceed on relatively large Pd particles at steady state. For Pd/NaHY, the products of this reaction have been reported to contain substantial amounts of branched higher hydrocarbons in addition to methane, methanol and dimethylether [9]. A strat-

egy is needed to prepare Pd carbonyl clusters with smaller nuclearity and to stabilize smaller Pd cores under reaction conditions. To this end, we have chosen to prepare  $\text{Pd}_6(\text{CO})_y$  clusters in zeolite 5A [10]. Both zeolites have similar sizes of supercages (or  $\alpha$ -cages) and sodalite cages (or  $\beta$ -cages), but the diameter of the cage windows is  $< 5 \text{ \AA}$  in 5A, whereas it is  $7.5 \text{ \AA}$  in NaY. Consequently, a shape-selectivity might be expected for CO hydrogenation leading to smaller molecules with zeolite 5A than with NaY. It is also conceivable that under reaction conditions smaller Pd particles will be stabilized in 5A than in NaY. In this paper, CO hydrogenation and variations of Pd particle size in Pd/5A are compared with Pd/NaY to probe the potential of catalyst synthesis by design.

## 2. Experimental

### 2.A. SAMPLE PREPARATION AND IN-HOUSE CHARACTERIZATION

Pd was introduced into zeolite 5A (Union Carbide, Ca form, lot No. 943084060054) by ion exchange at  $80^\circ\text{C}$  with  $0.01 \text{ M}$  solution of  $\text{Pd}(\text{NH}_3)_4(\text{NO}_3)_2$  (Johnson Matthey). The ion exchange was carried out for one week after which the sample was washed with doubly deionized water (DDW). Pd loading is  $2.1 \text{ wt\%}$ . Details of the ion exchange procedure have been described in a previous paper [10]. For simplicity, the fresh sample will be denoted as Pd-5A. The reduced sample will be referred to as Pd/5A. The general form of Pd/zeolite ( $T_C/T_R/t$ ) will be used to specify the pretreatment conditions, where  $T_C$  stands for the calcination temperature in  $^\circ\text{C}$ ,  $T_R$  for the reduction temperature in  $^\circ\text{C}$ , and  $t$  for the period of  $\text{H}_2$  reduction in min. In each calcination step, the heating rate was programmed at  $0.5^\circ\text{C}/\text{min}$  and the final  $T_C$  was maintained for 2 hr. In the reduction step, the heating rate was  $8^\circ\text{C}/\text{min}$ . Pd-NaY was also prepared by ion exchange of NaY (Linde, LZY-52) and  $\text{Pd}(\text{NH}_3)_4(\text{NO}_3)_2$ .

Static CO adsorption was performed at  $24^\circ\text{C}$ . Matheson-purity CO gas was used.

For FTIR, self-supporting wafers ( $20 \text{ mg}/\text{cm}^2$ ) of Pd/5A were used. A Nicolet 60SX single beam FTIR spectrometer of  $\text{cm}^{-1}$  spectral resolution was operated in transmission mode. The FTIR spectra in the CO absorption region are presented after subtracting the background of reduced Pd/5A. Other details of the in-situ IR cell and pretreatment conditions can be found elsewhere [10].

### 2.B. CO HYDROGENATION

CO hydrogenation was performed at  $290^\circ\text{C}$  and  $11 \text{ atm}$  using a  $\text{CO}/\text{H}_2$  mixture (Linde, UHP,  $\text{CO}:\text{H}_2 = 1$ ) in a stainless-steel continuous-flow fixed bed

reactor system (Max II Unit, Xytel Corp.). The total flow rate of the CO/H<sub>2</sub> mixture was maintained at 40 ml/min and 0.8 g of catalyst was used for each reaction giving a gas hourly space velocity of 1800 hr<sup>-1</sup>. The products were analyzed on-line with a HP 5890A GC equipped with a crosslinked methyl-silicon capillary column (i.d. = 0.2 mm, length = 50 m, He carrier) and FID.

### 3.C. CHARACTERIZATION BY EXAFS

For EXAFS measurements, samples were prepared ex-situ in a pyrex reactor with stopcock seals. After CO exposure at room temperature the samples were further purged with He and sealed. They were pelletized under a N<sub>2</sub> atmosphere in a glovebox and sealed in aluminum holders. The samples used in CO hydrogenation reaction were exposed to air and pelletized. The pellets were loaded into our EXAFS cell at the beam station. They were purged inside the cell with He at 200 °C for 20 min before H<sub>2</sub> reduction at the same temperature for 20 min. Subsequently, the samples were purged with He for 20 min and cooled in He.

As will be specified in the *Results* section, one sample that was calcined ex-situ at 500 °C was reduced with H<sub>2</sub> and purged with He in-situ at 250 °C. After EXAFS data collection, this sample was exposed to CO at 24 °C for 20 min, cooled to liquid N<sub>2</sub> temperature maintaining 1 atm CO pressure, and data were, again, collected.

EXAFS data, following the Pd K-edge at 24350 eV, were collected at X11A of National Synchrotron Light Source (NSLS) at Brookhaven National Laboratory. The ring energy is at 2.5 GeV. Typical filled current is 200 mA. The in-situ EXAFS results were obtained at CHESS, where the ring energy is at 5.0 GeV and current at 70 mA. The monochromator Si (111) crystal was detuned by 30% during data collection. A stainless-steel cell was used in transmission measurement at liquid nitrogen temperature. The detailed features of the cell and sample transfer procedure have been described in a previous publication [7].

EXAFS data were analyzed with the University of Washington software package. The  $k$  range from 4 to 14 Å<sup>-1</sup> in  $\chi$  data is used for Fourier transform. The  $R$  window used for inverse transform is from 2.0 to 3.0. A 0.025-mm Pd foil and PdO powder were used as reference structures for EXAFS data analysis. The coordination number ( $CN$ ) of Pd in the reference foil is taken as 12, and the Pd-Pd bond distance ( $R$ ) in the foil is assigned to 2.75 Å. In the PdO powder reference,  $CN = 4$  and  $R_{\text{Pd-O}} = 2.01$  Å.

## 3. Results

The FTIR spectra of Pd/5A(500/250/20) after CO exposure at 24 °C are shown in fig. 1. Two major bands are observed: a terminal CO at 2149 cm<sup>-1</sup> and

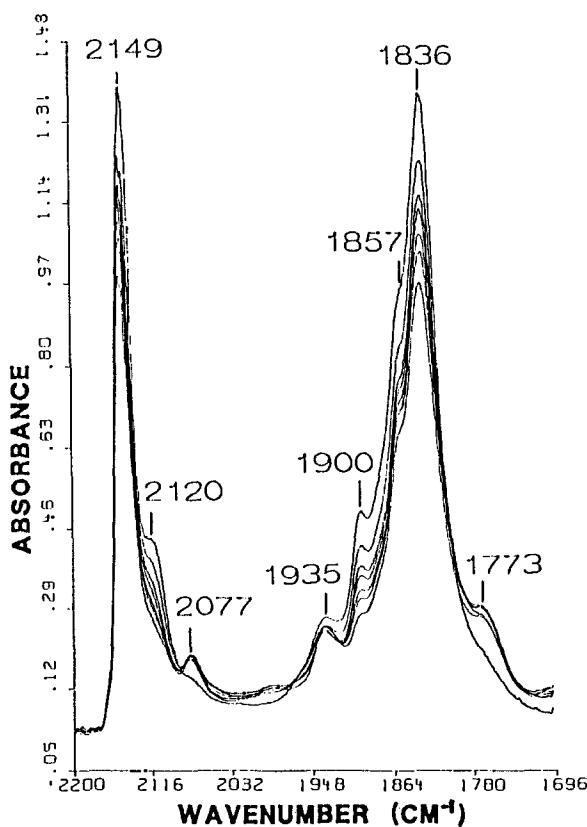


Fig. 1. FTIR spectra of Pd/5A(500/250/20) after admission of CO. The spectra in decreasing intensity correspond to purging in He for 10, 20, 30, 40, 60, 80, 120 min.

a triply-bridged CO band  $1836\text{ cm}^{-1}$ . During He purge, the intensities of these bands decrease. The FTIR spectra of Pd/5A after other pretreatment conditions show similar bands except for a slight shift in absorption wavenumber [10].

Shown in fig. 2 are the EXAFS  $k^2 \cdot \chi(k)$  functions of Pd/5A(500/250/20) (A) and Pd/5A(500/250/20) after in-situ CO exposure at room temperature for 20 min (B). The corresponding Fourier transforms are displayed in fig. 3 as A and B, respectively. They are presented here to qualitatively illustrate the Pd-CO shell. Fitting to the spectra would require not only a model compound for the Pd-C shell, but also a correction for the phase cancellation of Pd by the oxygen of CO ligands due to the focusing effect. This is, however, not a subject of concern in this paper.

The CO/Pd ratio obtained from CO chemisorption on Pd/5A(500/250/20) after subtracting physisorbed CO at corresponding pressure is shown in fig. 4. The ratio increases sharply at low CO pressure. At higher CO pressure, it varies from 1.2 to 1.6 over a broad range.

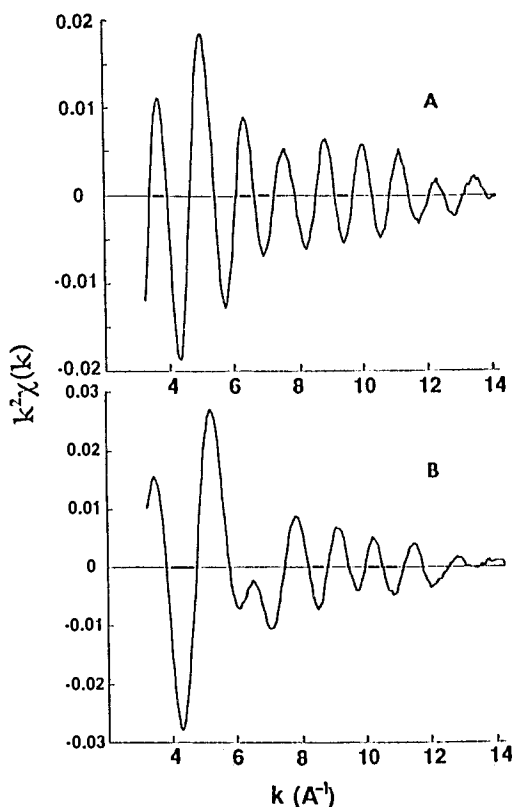


Fig. 2. EXAFS  $k^2 \cdot \chi(k)$  functions of (A) Pd/5A(500/250/20) and (B) Pd/5A(500/250/20) under 1 atm CO.

Fig. 5 compares the nuclearities of Pd/NaY and Pd/5A after CO exposure. Trace A is the  $k \cdot \chi(k)$  function of a Pd foil after reverse Fourier transform, windowed between  $R = 2.0$  and  $3.0 \text{ \AA}$ . Shown in trace B is the same function for Pd/NaY(500/200/20) after CO exposure at room temperature. Trace D (dotted line) is that of the Pd/5A(500/250/20) and trace C (inner solid line) was obtained after admission of CO to Pd/5A(500/250/20). The Pd/5A samples corresponding to trace C and D were prepared ex-situ. Any carbonyls formed were removed by purging with He after 20 min of CO exposure. Curve-fitting to trace B results in a coordination number of 6 for the Pd-Pd first nearest shell and  $R_{\text{Pd-Pd}} = 2.75 \text{ \AA}$ , as reported previously [7]. The coordination number obtained from trace C is 4 and  $R_{\text{Pd-Pd}} = 2.75 \text{ \AA}$ . Before CO admission, the coordination number is 3.5. In zeolite 5A, the increase of Pd nuclearity after admission of CO at room temperature is far less pronounced than in the case of zeolite Y [6,7].

After 24 hr of CO hydrogenation at  $290^\circ\text{C}$ , the average Pd particle size in zeolite NaY has greatly increased as evidenced by the amplitude of the Fourier

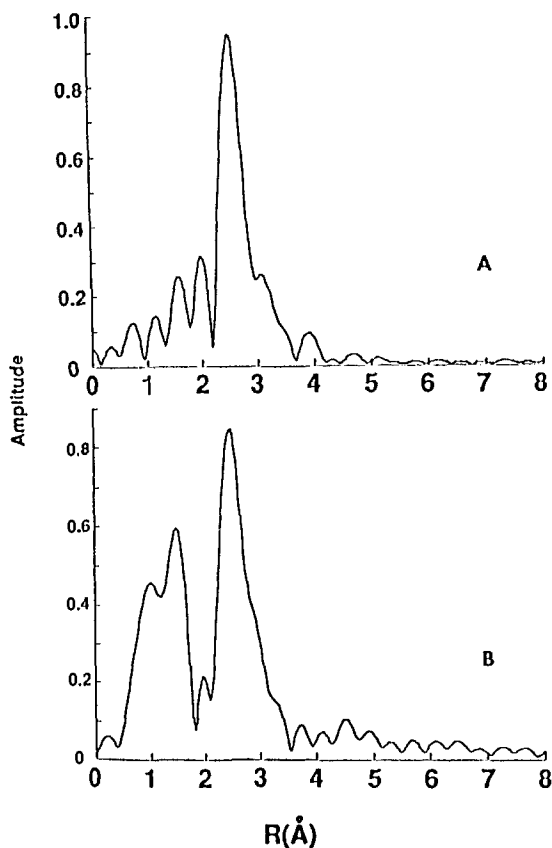


Fig. 3. Fourier transforms corresponding to (A) and (B) of fig. 2.

transform shown as trace **B** in fig. 6. For comparison, data for a Pd foil (trace **A**) are also shown. In contrast, the Pd/5A after reaction has not only a much smaller amplitude for the first Pd-Pd nearest shell and a much reduced amplitude for the second nearest Pd-Pd shell, but also the farther shells ( $R > 5 \text{ Å}$ ) for this sample are virtually absent. Clearly, the Pd particles after reaction are much smaller in 5A than in NaY. The results of curve-fitting to the reverse Fourier transforms of Pd/NaY and Pd/5A after reaction are shown in fig. 7 as traces **A** and **B**, respectively. The dotted lines represent experimental data and the solid lines are the theoretical fits. The coordination number ( $CN$ ) and interatomic distance  $R$  to the first Pd-Pd shell after catalytic reaction are 10.5 and 2.75 Å for Pd/NaY, respectively, but for Pd/5A, the values of  $CN$  and  $R$  are 6.5 and 2.75 Å, respectively.

The time-on-stream behavior for CO hydrogenation on Pd/5A(500/245/60) and Pd/5A(500/490/60) are shown in figs. 8 and 9, respectively. The selectivity on each catalyst is normalized with respect to the initial carbon production in  $\text{CH}_4$ . In contrast to Pd/NaY(500/350/60), where the production of higher

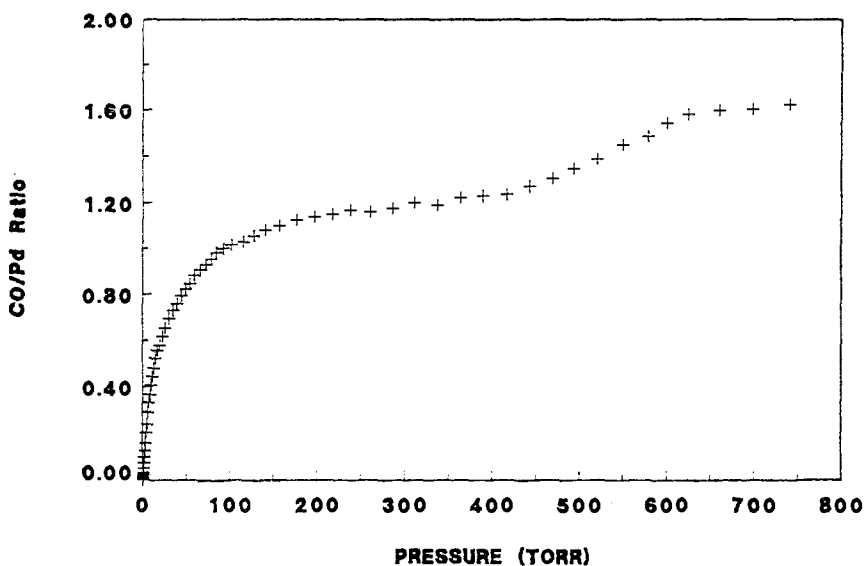


Fig. 4. CO/Pd ratio.

hydrocarbons is pronounced [11], Pd/5A produces only a negligible amount of  $C_{2+}$ . On this catalysts,  $CH_4$ ,  $CH_3OH$  and  $CH_3OCH_3$  are the only significant products. The CO hydrogenation selectivities of both Pd/5A(500/250/60) and Pd/5A(500/500/60) are plotted in fig. 10. The activity of Pd/5A is about twice that of Pd/NaY for CO hydrogenation at identical conditions [12], even though the Pd loading in Pd/5A is only about 60% of that in Pd/NaY.

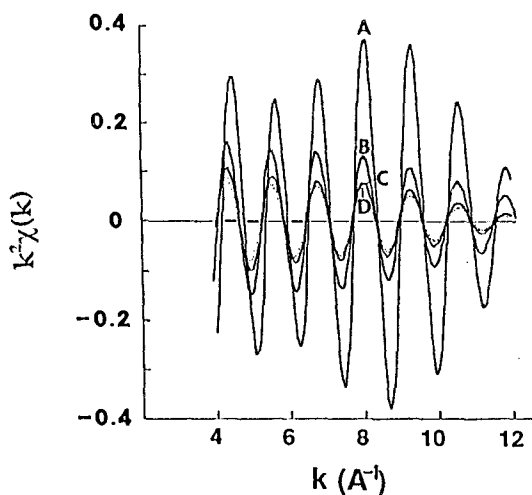


Fig. 5. EXAFS  $k^2\chi(k)$  functions of (A) Pd foil, (B) Pd/NaY(500/200/20) after CO exposure, (C) Pd/5A(500/250/20) after CO exposure (solid line) and (D) Pd/5A(500/250/20) before CO exposure (dotted line).

#### 4. Discussion

Since our EXAFS results give a coordination number of 4 for the Pd-Pd first nearest coordination shell in sample Pd/5A(500/250/20) after CO exposure, a Pd<sub>6</sub> octahedron is proposed for the core of the novel Pd cluster. In addition, the IR spectra (fig. 1) and the intense Pd-C coordination shell at 1.5 Å (fig. 3(B), phase shift (uncorrected)) strongly indicate the formation of a novel Pd carbonyl cluster. The combination of these results supports formation of Pd<sub>6</sub>(CO)<sub>x</sub> clusters in 5A. As shown in fig. 4, *x* varies greatly with *P*<sub>CO</sub> at low CO pressure. At higher *P*<sub>CO</sub>, it varies from 1.2 to 1.6 over a broad range of *P*<sub>CO</sub>. In the IR spectra of well-known Rh<sub>6</sub>(CO)<sub>16</sub> and Ir<sub>6</sub>(CO)<sub>16</sub> clusters, only terminal and

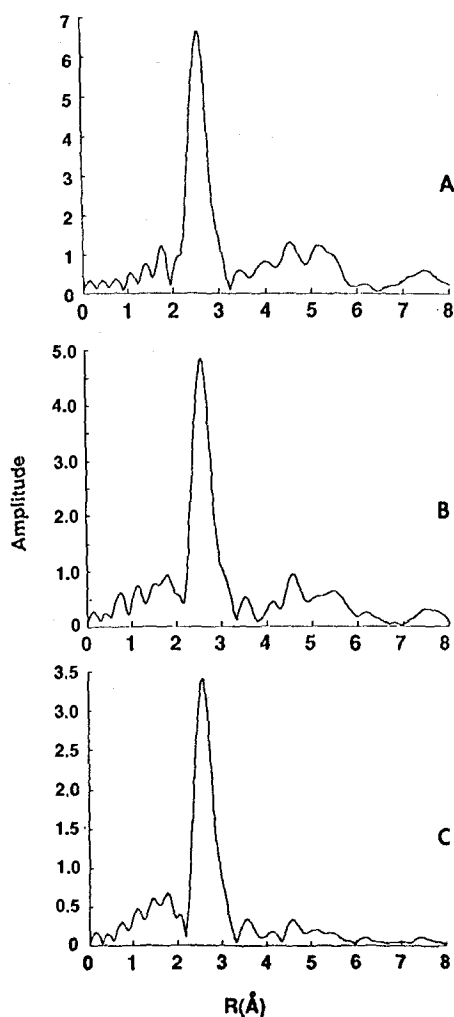


Fig. 6. Fourier transforms of EXAFS  $k^2 \cdot \chi(k)$  functions of (A) Pd foil, (B) Pd/NaY(500/200/20) after CO hydrogenation reaction and (C) Pd/5A(500/250/20) after CO hydrogenation reaction.



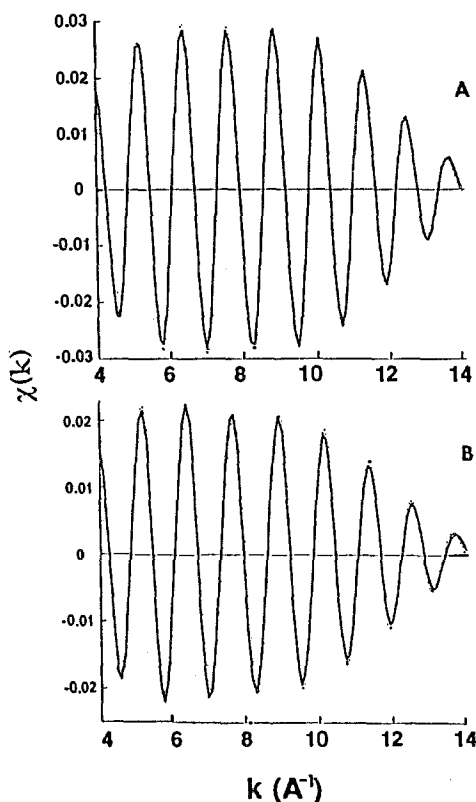


Fig. 7. Curve-fittings for the EXAFS  $\chi(k)$  functions of (A) Pd/NaY(500/200/20) after CO hydrogenation reaction and (B) Pd/5A(500/250/20) after CO hydrogenation reaction.

triply-bridged CO bands are observed [13]. For the novel  $\text{Pd}_6(\text{CO})_x$  cluster, we propose a similar structure. The IR spectrum of  $\text{Pd}_6(\text{CO})_x$  differs, however, from those of  $\text{Rh}_6(\text{CO})_{16}$  and  $\text{Ir}_6(\text{CO})_{16}$  in one important respect: in  $\text{Rh}_6(\text{CO})_{16}$  and  $\text{Ir}_6(\text{CO})_{16}$ , the ratio of terminal CO to triply-bridged CO is 2, in agreement with the ratio of the integrals of the two IR bands, but in  $\text{Pd}_6(\text{CO})_x$  the intensity of the triply-bridged CO band is higher than that of the terminal CO. Assuming that Wade's rules [14] apply, a cluster of  $\text{Pd}_6(\text{CO})_{13}$  might be proposed. The measured average CO/Pd ratio (fig. 4) is, however, lower than that predicted by Wade's rule. Whereas this might be due to the presence of larger clusters with much lower CO/Pd ratios, the applicability of Wade's rules for Pd carbonyl clusters is questionable because the Pd-CO bond is weaker than the Pd-Pd bonds. Still, our FTIR spectrum can be rationalized on the basis of Wade's rules: In a  $\text{Pd}_6(\text{CO})_{13}$  cluster, 8 CO ligands should be assigned to the triply-bridged CO coordinated to the 3 Pd atoms comprising each face of the  $\text{Pd}_6$  octahedron and the remaining 5 CO ligands are terminally coordinated to one Pd atom. This 8/5 ratio is consistent with the intensity ratio of the observed

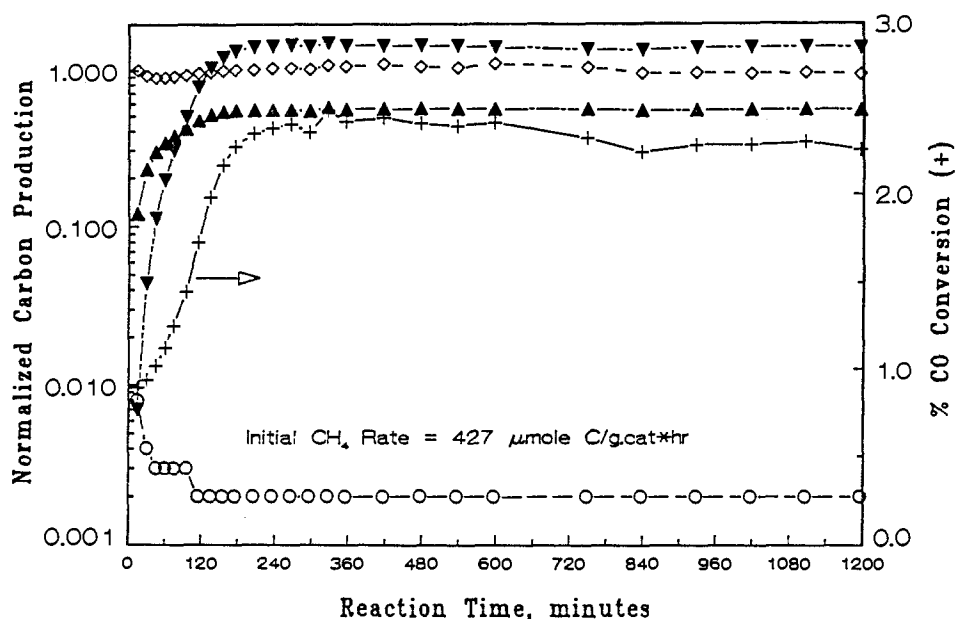


Fig. 8. Product yields during CO hydrogenation over Pd/5A(500/245/60) vs. time on stream. Reaction temperature:  $290 \pm 2^\circ\text{C}$ ; pressure:  $11.1 \pm 0.2\text{ atm}$ ; GHSV:  $1950 \pm 50\text{ hr}^{-1}$ ; and  $\text{CO}/\text{H}_2$ : 1.  $\diamond$ --- $\diamond$   $\text{CH}_4$ ;  $\circ$ --- $\circ$   $\text{C}_{2+}$  hydrocarbons;  $\blacktriangle$ --- $\blacktriangle$   $\text{CH}_3\text{OH}$ ;  $\blacktriangledown$ --- $\blacktriangledown$   $\text{CH}_3\text{OCH}_3$ ; and  $+$ — $+$  %CO conversion.

FTIR bands. This assignment leaves one Pd in the octahedron uncoordinated. It is very likely that this Pd atom is bonded to  $\text{Ca}^{2+}$  ions or to protons generated during the reduction of Pd. In view of the fact that the terminal CO band has a significant blue shift with respect to that on the bulk Pd [15,16], this indicates an electron deficiency for the Pd core. In our previous work on Pd/NaHY and Pd/MgHY, a blue shift of terminal CO groups in  $\text{Pd}_{13}(\text{CO})_x$  clusters has been attributed to interaction of Pd with zeolitic protons [4,5,8]. The weaker bands in fig. 1 are likely due to different coordination such as doubly-bridged CO or perhaps due to the presence of some of larger clusters. A variation of  $x$  in  $\text{Pd}_6(\text{CO})_x$  as determined by the CO chemisorption isotherm is also observed in the IR spectra; during He purging, the intensity of the CO absorption bands decreases. This observation shows that bonds between Pd and CO ligands are rather weak. This is in contrast to Rh carbonyl clusters in zeolite Y, where the intensity of the CO bands is not changed by He purging [17].

For Pd/NaY, the nuclearity after mild reduction depends strongly on the calcination and reduction temperatures, as has been shown by our previous EXAFS studies [6–8]. For the samples calcined at  $500^\circ\text{C}$ , the Pd particle sizes vary from monoatomic to octahedral as the reduction temperature increases from  $200^\circ\text{C}$  to  $350^\circ\text{C}$ . The stability of such small Pd nuclei at these temperatures has been attributed to the anchoring effect of protons. Admission of CO to

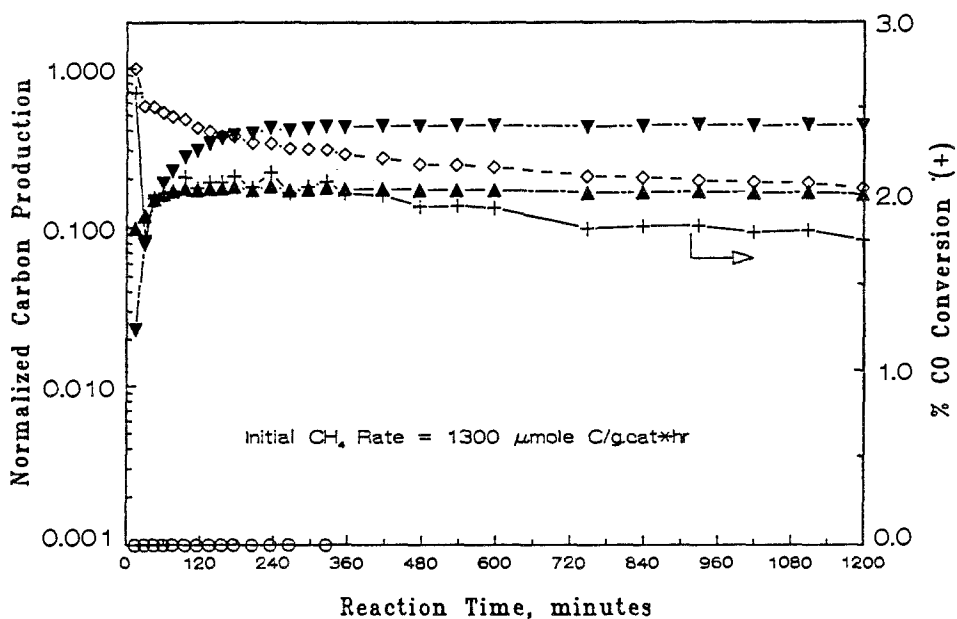


Fig. 9. Product yields during CO hydrogenation over Pd/5A(500/290/60) vs. time on stream. Reaction temperature:  $288 \pm 2^\circ \text{C}$ ; pressure:  $11.2 \pm 0.2 \text{ atm}$ ; GHSV:  $2100 \pm 50 \text{ hr}^{-1}$ ; and  $\text{CO}/\text{H}_2$ : 1.  $\diamond$ --- $\diamond$   $\text{CH}_4$ ;  $\circ$ — $\circ$   $\text{C}_{2+}$  hydrocarbons;  $\blacktriangle$ --- $\blacktriangle$   $\text{CH}_3\text{OH}$ ;  $\blacktriangledown$ --- $\blacktriangledown$   $\text{CH}_3\text{OCH}_3$ ; and  $+$ — $+$  %CO conversion.

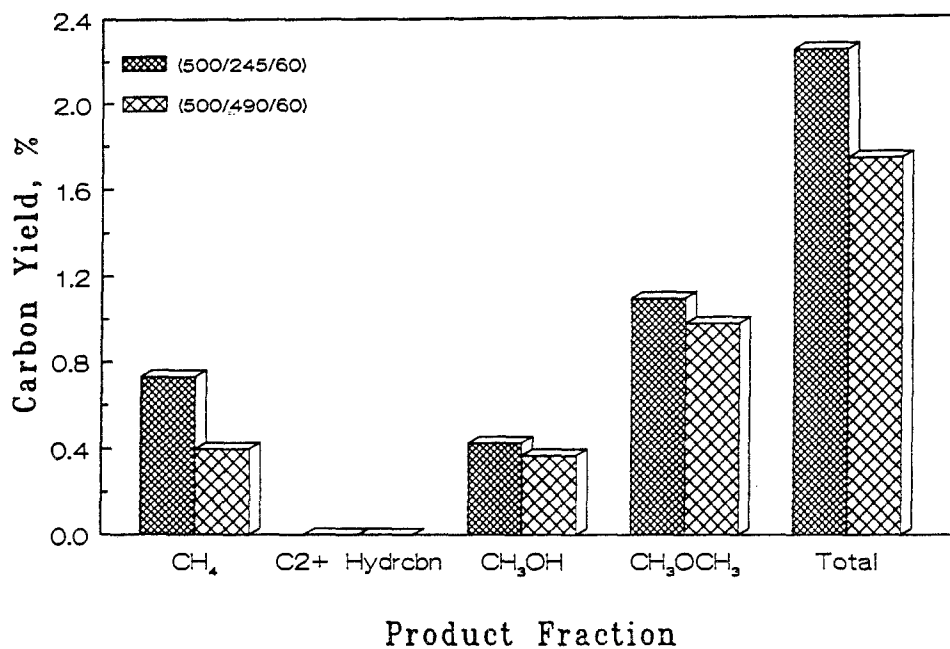


Fig. 10. Carbon yields of products at steady state in CO hydrogenation over Pd/5A catalysts.

the reduced Pd/NaY weakens the interaction between Pd and proton, inducing migration and coalescence of primary Pd carbonyl.

A comparison in fig. 5 of the EXAFS functions Pd/NaY(500/200/20) and Pd/5A(500/250/20) after admission of CO at room temperature clearly demonstrates the decisive effect of the window size on the formation of Pd carbonyl clusters of different nuclearity. We have shown with EXAFS spectroscopy that Pd<sub>13</sub>(CO)<sub>x</sub> clusters always prevail in NaY supercages upon exposing mildly reduced Pd/NaY to CO at room temperature [6–8]. In NaY, the Pd core of Pd<sub>13</sub>(CO)<sub>x</sub> has a diameter of 8.2 Å, assuming spherical geometry of a cubooctahedron or an icosahedron. Its migration is restricted by the 7.5 Å supercage window diameter even if it sheds off some of its CO ligands. However, for zeolite 5A the supercage window is much smaller viz. < 5 Å, even though the diameter of the supercage in NaY and 5A is not significantly different. As a consequence, the Pd core ceases to grow in 5A under CO atmosphere at room temperature when Pd<sub>6</sub>(CO)<sub>x</sub> is formed. This comparison therefore leads to the conclusion that for the final carbonyl cluster size, although the cage sizes of NaY and 5A are quite similar, the geometric limitation of the zeolite cage window is critical.

In a previous study, it has been shown that the process of migration and coalescence of Pd carbonyl clusters is not reversed by removal of CO [7]. On the contrary, H<sub>2</sub> purge to 200 °C following admission of CO to Pd/NaY at room temperature leads to further growth of Pd particles. Under CO hydrogenation conditions with Pd/NaY, e.g., at 220 °C, the Pd particle size was found to increase drastically. CO FTIR of the catalyst after reaction showed a spectrum characteristic of large Pd particles [11]. The coordination number of 10.5 of the first Pd-Pd shell for the Pd/NaY after reaction at 290 °C indicates that the Pd particles have grown too large for EXAFS to be sensitive enough to determine its actual size. The comparable amplitudes of Pd-Pd distances extending to 8 Å between Pd/NaY after reaction and Pd foil further confirm the formation of large Pd particles under reaction condition. The X-ray diffraction pattern of this catalyst also suggests the presence of Pd particles larger than 60 Å [12].

It is therefore quite remarkable that very small Pd particles survive in the α-cages of zeolite 5A after reaction, as evidenced by: (1) the small coordination number (6.5) of the first Pd-Pd nearest shell based on the curve-fitting of the EXAFS function; (2) the absence of Pd-Pd bonds in the EXAFS Fourier transform at distances farther than the second nearest neighbors; and (3) the absence of X-ray diffraction peaks indicating large Pd particles.

The stabilization of small Pd particles results in a higher steady state activity for CO hydrogenation in zeolite 5A in comparison to Pd/NaY at identical conditions [12]. The decline in activity for Pd/NaY catalysts has been ascribed to two causes: agglomeration of Pd particles and formation of a Pd-C solution. The absence of agglomeration in Pd/5A is ascribed to its window size of less than 5 Å. An induction period in the production of CH<sub>3</sub>OH and CH<sub>3</sub>OCH<sub>3</sub> of

about 3 hr for Pd/5A(500/245/60) and (500/490/60) can be explained by the initial increase of Pd nuclei size under reaction condition as shown by EXAFS. In view of the large demand for oxygenates in industries particularly in the future fuel market, the high selectivity of methanol and dimethylether of Pd/5A catalysts might be of relevance. The selectivity for methanol and dimethylether in 5A is likely due to steric effects. While molecular shuttling in Pd/NaHY is unrestricted by the large supercage windows, the growth of C<sub>2+</sub> hydrocarbon molecules is sterically limited in Pd/5A. It may also be relevant that the Brønsted acidity is lower in 5A than in NaHY.

## Acknowledgments

We thank Professor E. Stern of University of Washington for kindly donating his EXAFS package. Financial support by the National Science Foundation Grant Number CTS11184 and a grant-in-aid of the Engelhard Corporation are gratefully acknowledged.

## References

- [1] T.J. Lee and B.C. Gates, *Catal. Lett.* 8 (1991) 15.
- [2] L.F. Rao, A. Fukuoka and M. Ichikawa, *J. Chem. Soc., Chem. Commun.* (1988) 458.
- [3] L.L. Sheu, H. Knözinger and W.M.H. Sachtler, *Catal. Lett.* 2 (1989) 129.
- [4] L.L. Sheu, H. Knözinger and W.M.H. Sachtler, *J. Am. Chem. Soc.* 111 (1989) 8125.
- [5] L.L. Sheu, H. Knözinger and W.M.H. Sachtler, *J. Mol. Catal.* 57 (1989) 61.
- [6] Z. Zhang, H. Chen, L.L. Sheu and W.M.H. Sachtler, *J. Catal.* 127 (1991) 213.
- [7] Z. Zhang, H. Chen and W.M.H. Sachtler, *J. Chem. Soc., Faraday Trans. I* 87 (9) (1991) 1413.
- [8] Z. Zhang, T.T. Wong and W.M.H. Sachtler, *J. Catal.* 128 (1991) 13.
- [9] F.A.P. Cavalcanti, C. Dossi, L.L. Sheu and W.M.H. Sachtler, *Catal. Lett.* 6 (1990) 289.
- [10] Z. Zhang and W.M.H. Sachtler, *J. Mol. Catal.*, in press.
- [11] F.A.P. Cavalcanti, C. Dossi, L.L. Sheu and W.M.H. Sachtler, *Catal. Lett.* 6 (1990) 289.
- [12] F.A.P. Cavalcanti and W.M.H. Sachtler, in preparation.
- [13] L. Garlaschelli, S. Martinengo, P.L. Bellon, F. Demartin, M. Manassero, M.Y. Chiang, C.Y. Wei and R. Bau, *J. Am. Chem. Soc.* 106 (1984) 6664.
- [14] C.M. Lukehart, *Fundamental Transition Metal Organometallic Chemistry* (Brooks/Cole Publishing Company, Monterey, California, 1985).
- [15] A.M. Bradshaw and F. Hoffmann, *Surf. Sci.* 52 (1975) 449.
- [16] A. Palazov, C.C. Chang and R.J. Kokes, *J. Catal.* 36 (1975) 338.
- [17] T. Wong, Z. Zhang and W.M.H. Sachtler, *Catal. Lett.* 4 (1990) 365.